24th COBEM - 2017

24th ABCM International Congress of Mechanical Engineering
December 3-8, 2017, Curitiba, PR, Brazil

RAPID SOLIDIFICATION AND CHARACTERIZATION OF Ni-*x*Nb BINARY ALLOYS

Katherine Martínez O.
Graduation Program in Materials Science and Engineering (PPG-CEM), Universidade Federal de São Carlos (UFSCar), Rod. Washington Luís, km 235, 13565-905, São Carlos – SP, Brazil
kathemartinezorozco@gmail.com

Carlos A. D. Rovere
Claudio S. Kiminami
Conrado R. M. Afonso
Department of Materials Engineering (DEMa), Universidade Federal de São Carlos (UFSCar), Rod. Washington Luís, km 235, 13565-905, São Carlos – SP, Brazil
carlosdrovere@gmail.com; kiminami@power.ufscar.br; conrado@ufscar.br

Abstract. *In this work Ni-xNb (x = 10, 15, 20, 30, 40, 45, 52 and 57 wt%Nb) alloys were rapidly solidified through arc-melting in order to compare equilibrium phases and metastable phases formed in quenched condition. The characterization was realized in order to confirm phases formed and the mechanical property was evaluated using Vickers microhardness.*

Keywords: *Rapid solidification, Ni-based alloys, metastable phases, characterization.*

1. INTRODUCTION

Ni-based alloys can be used in several advanced applications, such as aerospace industry, land-based turbine disks, nuclear power plants, and petrochemical engineering (Donachie, 2002). A great variety of Ni-Cr-Fe-based superalloys were developed, among them a widely used is the Inconel 718 as a precipitation-strengthened alloy with alloying additions of Mo, Nb, Ti, and Al (Davis, 2000). On the other hand, Ni-Nb binary and multicomponent alloys can be classified as bulk metallic glasses (BMG), starting with the best binary glass former alloy $Ni_{62}Nb_{38}$ (at%) with 2 mm glassy diameter cylinder diameter (Inoue, 2011), up to 5 mm for $Ni_{59}Zr_{19}Ti_{11}Nb_6Si_3Sn_2$ (at%). In particular, Ni-based BMG show excellent mechanical properties (e.g., high strength and good ductility), high thermal stability and excellent corrosion resistance (Afonso, 2012). Additionally, ferromagnetic Fe-, Co-, and Ni-based multicomponent amorphizable alloys can reach glassy state in micrometric powder (size range of a few microns up to 500 μm) when submitted to rapid solidification processing routes such as gas atomization using nitrogen or argon inert gases (Inoue, 1988),(Afonso, 2007), copper mold casting in millimeters range pieces (Afonso, 2012) laser cladding coatings of hundreds of microns thick (Gargarella, 2014) and ribbons obtained by melt-spinning (May, 2004) imposing cooling rates from 10^3 to 10^6 K/s. Usually crystalline Ni-based alloys tends to form Ni-fcc matrix and metastable γ" Ni_3Nb intermetallic phase body centered tetragonal (bct), or orthorhombic δ precipitates of Ni_3Nb, and undesirable Cr_2Nb Laves phase, while equilibrium phases formed for binary $Ni_{62}Nb_{38}$ (at%) relies on orthorhombic δ-Ni_3Nb and μ-Ni_6Nb_7 intermetallic phases (Donachie, 2002). In literature, there is a lack of studies of intermetallic phase´s formation in rapidly solidified Ni-Nb binary systems, regarding metastable phases and the existence of a metastable coupled binary phase diagram. One these had been the undercooled eutectics in Ni-Nb melts, by electromagnetic levitation technique, in order to study the microstructures formed for the two eutectics of these system, under certain undercooling conditions (Leonhardt, 1999). Most of the alloys studied relies on commercial Ni-Cr-based superalloys such as Inconel 625 and 718 among others with Nb contents up to 5.5 wt% and bulk metallic glasses with high contents of Nb around 30 to 40 at. % (Special Metals, 2013), but usually in ternary systems and multicomponent alloys. In this way, the aim of this work is to obtain and to characterize rapidly solidified Ni-*x*Nb (x = 10, 15, 20, 30, 40, 45, 52 and 57 wt. %) alloys through arc-melting in order to compare equilibrium phases and metastable phases formed in quenched condition.

2. EXPERIMENTAL PROCEDURE

The samples of Ni-*x*Nb (x = 10, 15, 20, 30, 40, 45, 52 and 57 wt% Nb) were produced by arc-melting with argon atmosphere, in the form of 18g ingots using pure elements Ni pieces 99.9% and Nb rods 99.95% purity. The chemical compositions were chosen using equilibrium phase diagram as a reference, taking in count the phase's formation. This diagram is shown in Fig. 1, and colored lines represents the different compositions (Davis, 2000). Samples were cutted cross-sectionally and characterized by scanning electron microscopy (SEM) with a FEI Inspect S50 coupled to X-ray energy dispersive spectroscopy (EDS), X-ray diffraction (XRD) was performed using a Siemens D5005 diffractometer and Cu-K_α radiation in order to confirm the formation of equilibrium and non-equilibrium phases. The samples also were subjected to Vickers microhardness (HV) measurements performed with a Shimadzu HMV-G 20ST equipment with pyramid-shaped diamond indenter with a load of 300 g for 15 s with the aim of correlate these results with microstructure and XRD patterns.

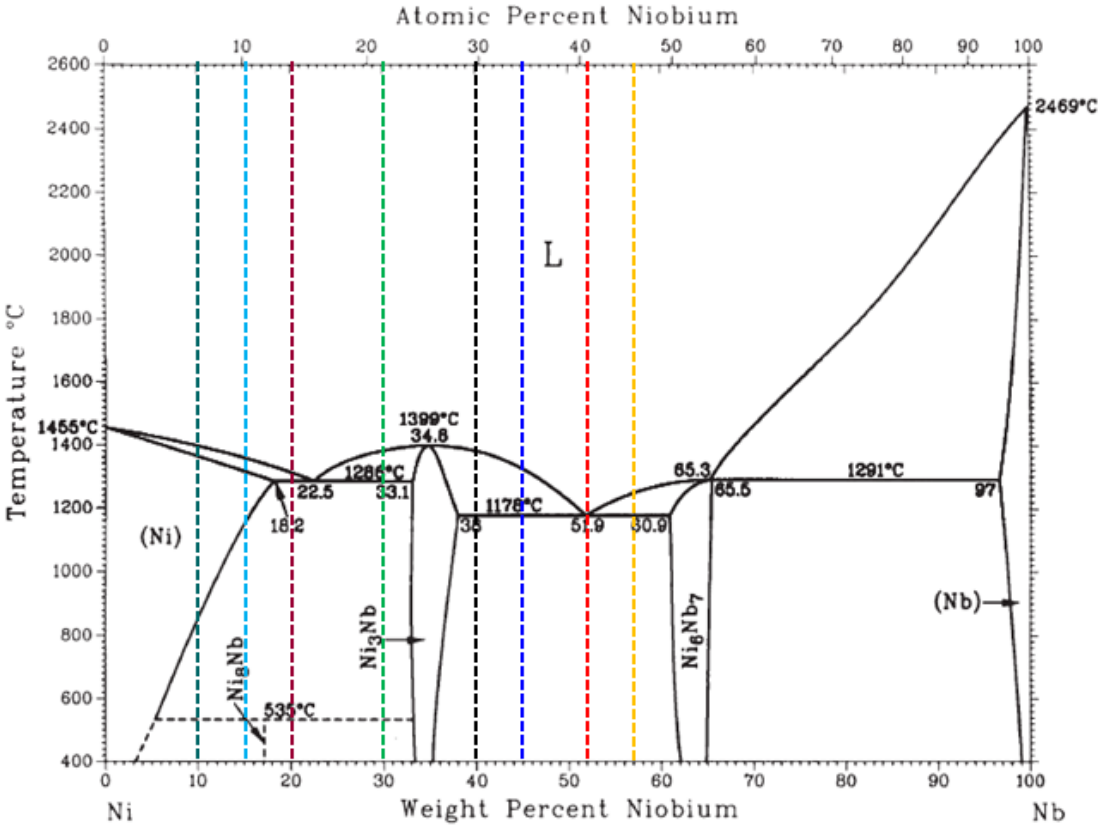

Figure 1: Binary diagram showing colored lines for Ni-xNb alloys studied in this work: x=10, 15, 20, 30, 40, 45, 52 and 57 (wt%Nb) alloys.

3. RESULTS AND DISCUSSION

3.1 X-ray Diffraction (XRD)

The XRD result shows that the equilibrium phases were formed for Ni-*x*Nb (x = 10, 15 and 20 wt% Nb) with Ni-fcc matrix and δ-Ni_3Nb intermetallic phase. XRD patterns of hypoeutectic Ni-Nb alloys did not confirmed the identification of metastable Ni_8Nb phase as depicted in Fig. 2 (left). Further TEM (transmission electron microscopy) analysis is needed in order to confirm this phase in the case of nanoscale precipitation. According to Quist and Wekken, the nucleation and growth of this phase occurs under a critical temperature (500°C) and requires large concentration of excess vacancies, produced either by rapid quenching or charged-particle radiation (Chen, 2006).

As observed in Fig. 2 (right), the equilibrium phases δ-Ni_3Nb and μ-Ni_6Nb_7 patterns were clearly identified in Ni-40Nb, Ni-45Nb, Ni-52Nb and Ni-57Nb (wt. %) alloys with exception of Ni-30Nb where just δ-Ni_3Nb was detected.

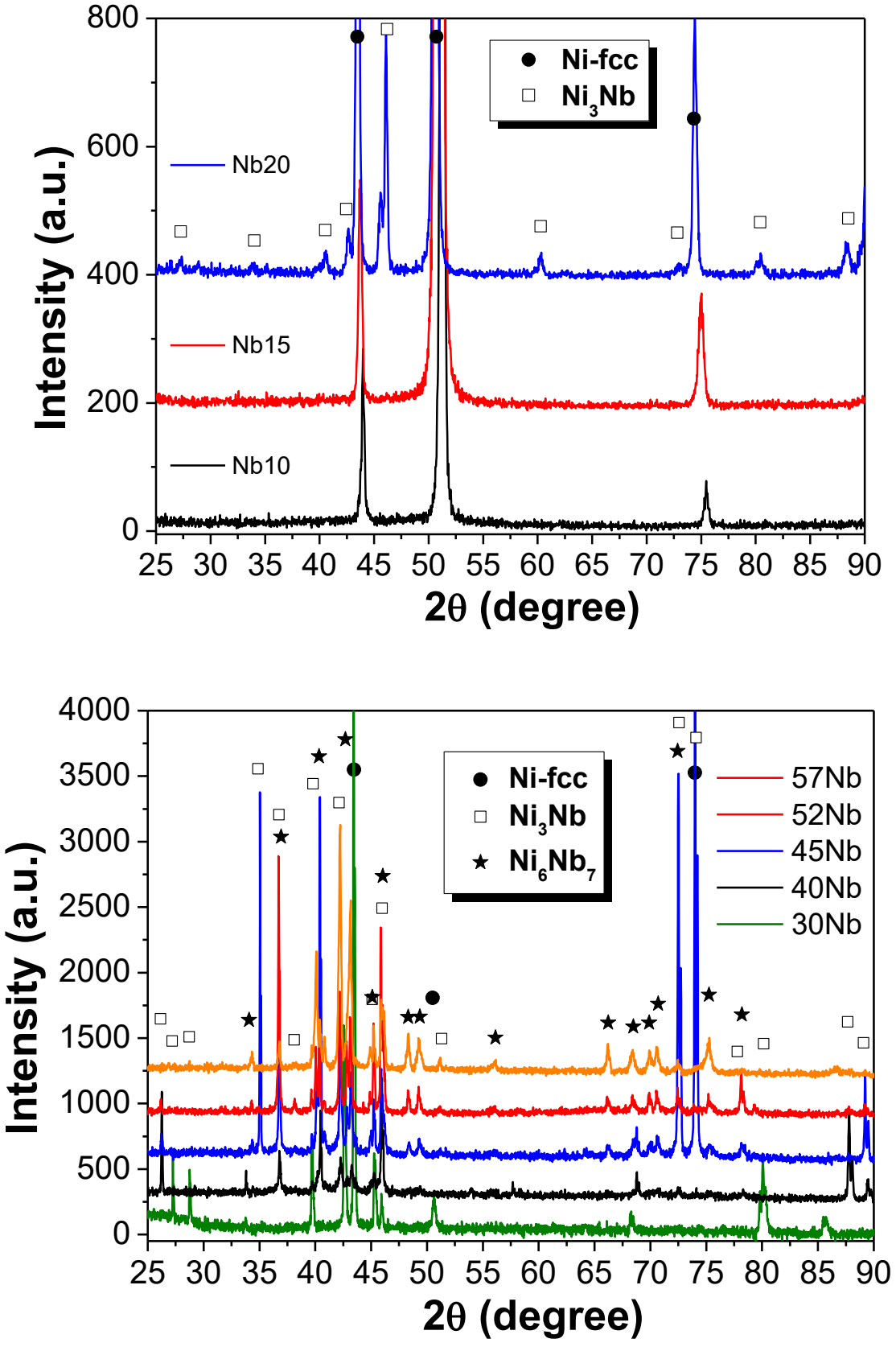

Figure 2: XRD patterns for arc-melting samples rapidly solidified alloys (left) Ni-10Nb, Ni-15Nb and Ni-20Nb (wt. %) and (right) Ni-30Nb, Ni-40Nb, Ni-45Nb, Ni-52Nb and Ni-57Nb (wt. %) alloys.

3.2 Scanning Electron Microscopy (SEM)

Figure 3. shows scanning electron microscopy (SEM) images in backscattered electrons (BSE) mode for arc-melted Ni-10Nb Fig. 3 (a, d), Ni- 15Nb Fig. 3 (b, e) and Ni-20Nb Fig. 3 (c, f), rapidly solidified alloys showing dendritic growth, with Nb content increased dendritic microstructure appears refined, although Ni-10Nb and Ni-15Nb does not exhibit interdendritic precipitates, meanwhile in Ni-20Nb was observed an intermetallic precipitate δ-Ni_3Nb (clear phase) with irregular morphology as shown in Fig. 3 (c, f). A needle-like shape precipitate is also formed, suggesting the presence of another different phase, not identified in DRX pattern.

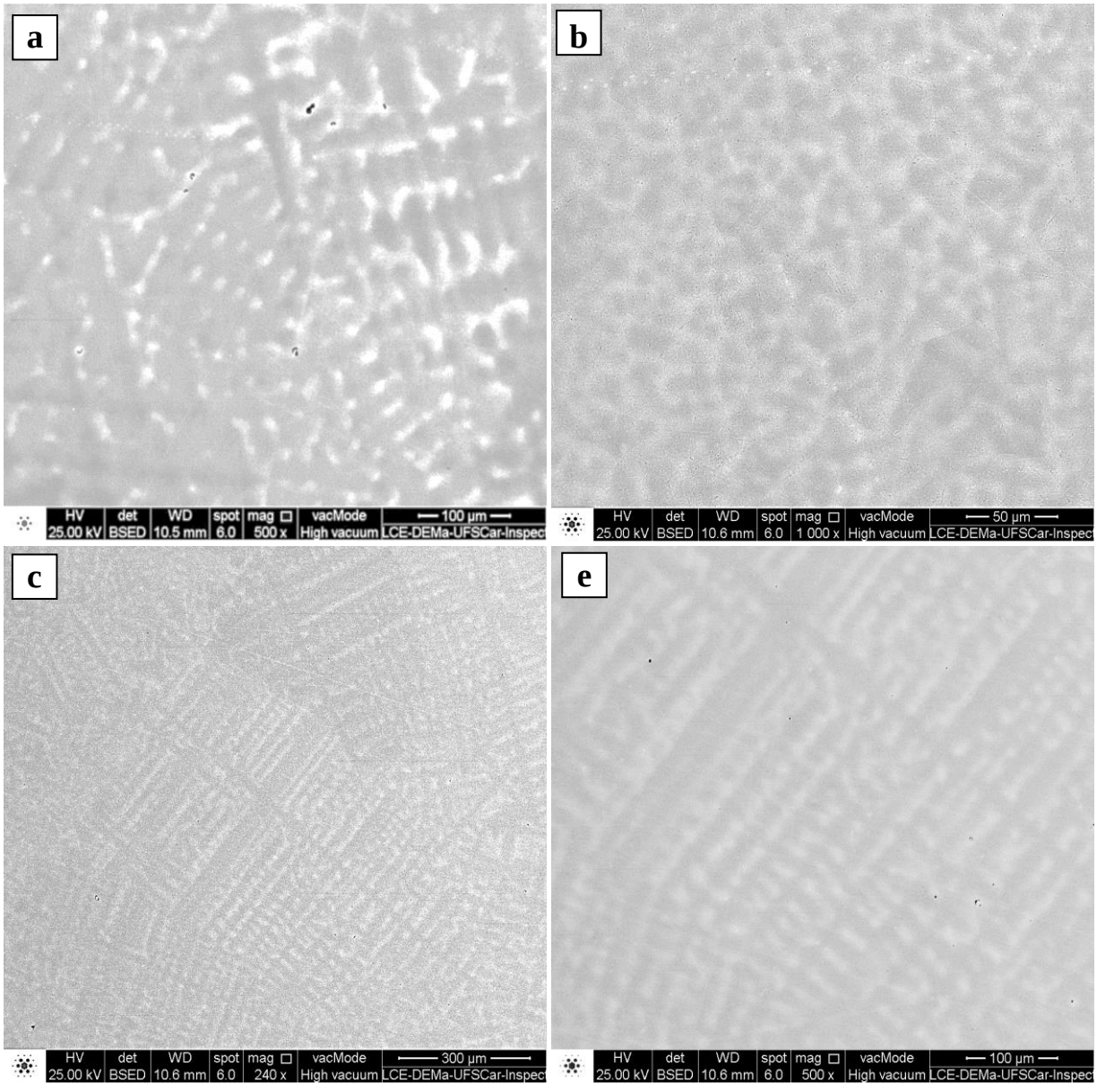

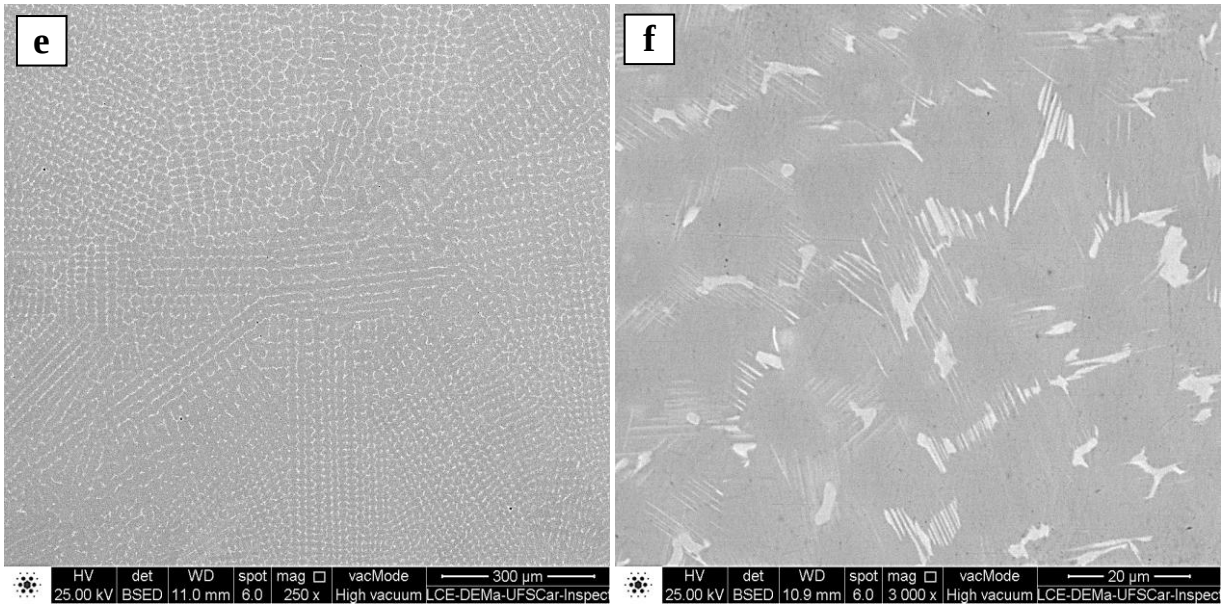

Figure 3: SEM images in BSE mode for arc-melted (a, b) Ni-10Nb, (c, d) Ni-15Nb and (e, f) Ni-20Nb (wt%) rapidly solidified alloys, in lower and higher magnifications.

With an increase of Nb content, morphology starts to change drastically. As depicted in Fig. 4 (a) Ni-30Nb micrograph, the morphology exhibits transitional growing from cellular to dendritic, with higher fraction of a clear phase identified as δ-Ni_3Nb growing in the depleted Ni-fcc matrix. In Fig. 4 (b) is observed Ni-40Nb a composition in which Ni-fcc was already replaced for Ni_3Nb and appears to be higher fraction as a matrix with eutectic Ni_3Nb + Ni_6Nb_7 dispersed on it. EDS analysis shows 50.73 wt. % of Nb, a result that is in agreement with binary Ni-Nb phase diagram. A similar behavior was found in Ni-45Nb sample, as illustrated in Fig. 4 (c, d), but with a coarser eutectic and less fraction of Ni_3Nb as matrix. Ni-30Nb, Ni-40Nb and Ni-45Nb morphologies are similar to $Ni_{59}Nb_{35}Sn_6$ alloy copper mold-cast (Catto, 2017). In Ni-52Nb sample the microstructure, the second eutectic in the system (51.9 wt. %), exhibits almost entirely the eutectic phase as shown in Fig. 4 (e), besides another phase diamond-like shape appears dispersed on the eutectic matrix.

According to EDS analysis, this phase was identified as Ni_6Nb_7 and presents a 70.2%Nb (wt.%), which is a value quite further from the eutectic composition indicating supersaturation of Nb, this can be explained due to the rapid solidification that promotes the precipitation of this phase prior to eutectic, out of equilibrium conditions. The eutectic Nb percentage was quantified in 49.4% (wt.%), and is left-displaced from eutectic value on the equilibrium diagram, this also occurred because of rapid solidification rates which can alter solubility behavior as illustrated in Fig. 5. explained by metastable extensions of *liquidus* lines (Leonhardt, 1999). It is important to pointed out that Ni-52Nb is an important glass former (Minouei, 2017)(Koch, 1983), and it was observed sub-micrometric size for the eutectic. Sample with Ni-57%Nb presents a Ni_6Nb_7 matrix (clear phase) with even higher fraction of eutectic dispersed on it. EDS results shows 58.74% Nb content in this phase, meanwhile eutectic composition was observed to have 49.06%Nb, a value also left-displaced from equilibrium eutectic composition as observed in Ni-52%Nb sample.

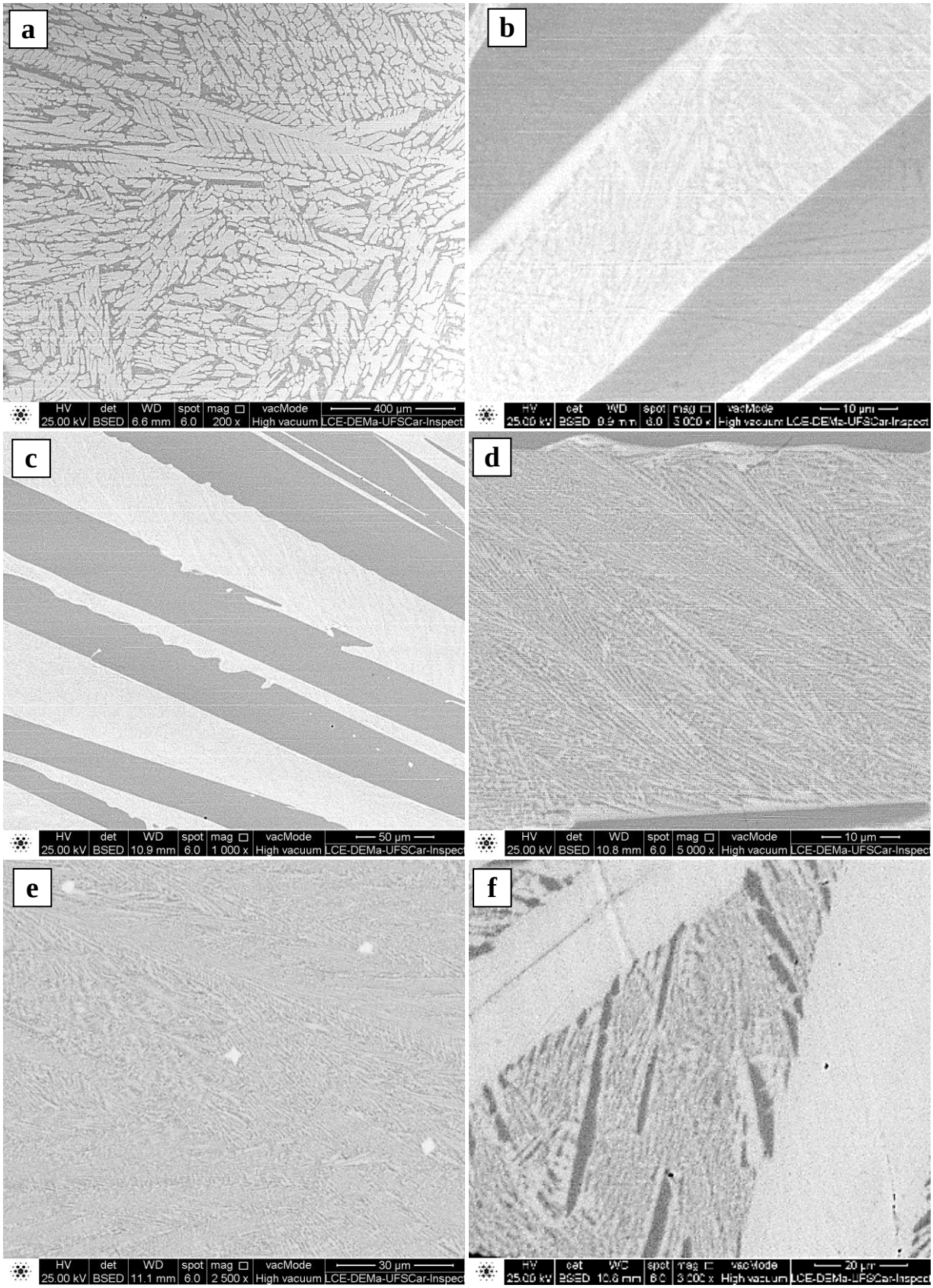

Figure 4: SEM images in BSE mode for arc-melted (a) Ni-30Nb, (b) Ni-40Nb, (c, d) Ni-45Nb, (e) Ni-52Nb and (f) Ni-57Nb (wt%) rapidly solidified alloys.

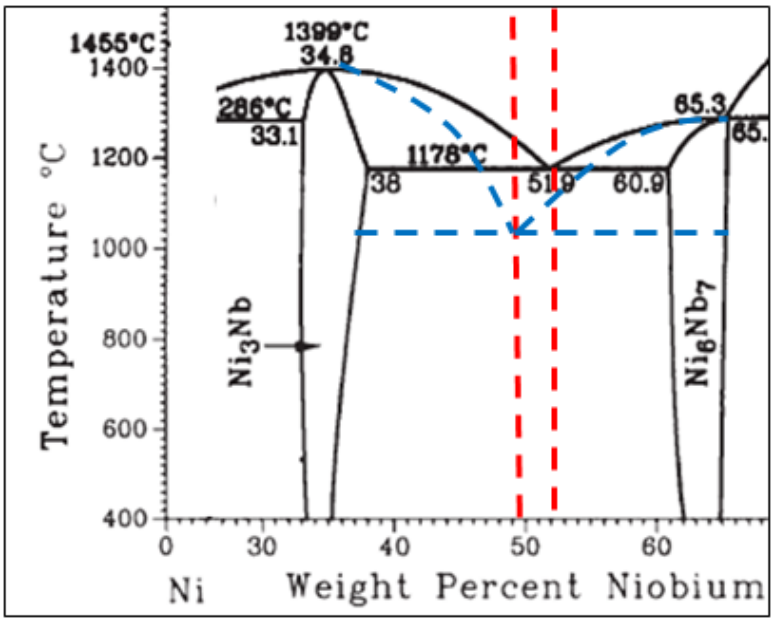

Figure 5: Equilibrium diagram showing displacement of coupled eutectic composition due to high coolig rates during rapid solidification by copper mold casting.

3.3 Hardness Vickers (HV), chemical composition, XRD and SEM correlation.

Table 1 summarized the results of Vickers microhardness test for arc-melting Ni-Nb rapidly solidified alloys. As depicted in Fig. 5, it can be observed that there is a significant increasing of Vicker microhardness values with increment in Nb addition, which is an expected behavior since Nb is one of the principal solid solution strengtheners in super alloys (Davis, 2000). It must be pointed out that hardness value is significantly high in Ni-15%Nb alloy (193 ± 2HV) in comparison with commercial superalloy Inconel 625 (179 HV) which Nb content is about 3.15-4.15 wt.% (Special Metals, 2013). Surprisingly, Ni-20Nb alloy ($Ni_{86}Nb_{14}$ in at.%) resulted in a Vicker microhardness value of 306 ± 6, much higher than that of commercial Ni-based superalloy Inconel 625, that hardness increasing can be attributed to combination of phases formed according to XRD and SEM characaterization, indicating formation of hard Ni_3Nb (irregular morphology) and Ni_8Nb (nanometric scale needle shaped) intemetallic phases dispersed in and surrounding the Ni-fcc cellular matrix growth sizing around 15 μm in diameter.

Besides increase of Nb content, strengthened occurs due to refinement of γ (Ni-fcc) dendritic microstructure and subsequent formation of δ-Ni_3Nb and μ- Ni_6Nb_7 intermetallic phases. On the other hand, XDR analysis for Ni-*x*Nb (x = 30, 40, 45, 52 and 57 wt,%Nb) shows that Ni-fcc fraction decreases with the addition of Nb content and improves the formation of eutectic Ni_3Nb + Ni_6Nb_7 as depicted in Fig. 4. This can be verified in the XRD patterns showed previously in Fig. 2 where peaks of Ni-fcc appears with lower intensity anytime according to the Nb percentage increment.

As presented in Table 1, Vickers microhardness results for 52%wt.Nb alloy (863±34 HV) is higher than 57wt.%Nb alloy (758±44 HV). This can be explained due to precipitation of an additional fractions of diamond-like Ni_6Nb_7 intermetallic phase, which is richer in Nb, while this behavior was not observed in 57wt.%Nb alloy, only constituted by lower fraction of eutectic matrix composed by Ni_3Nb+ Ni_6Nb_7 intermetallic phases.

Table 1 – Values of Vickers microhardness measured for arc-melting Ni-Nb rapidly solidified alloys correlated with SEM and chemical composition.

Alloy (wt. %)	Alloy (at. %)	Phases (SEM)	Hardness Vickers (HV)
Ni-10Nb	$Ni_{94}Nb_6$	↑ Ni-fcc	179 ± 8
Ni-15Nb	$Ni_{90}Nb_{10}$	↑ Ni-fcc + Ni_3Nb ↓	193 ± 2
Ni-20Nb	$Ni_{86}Nb_{14}$	Ni-fcc + Ni_3Nb + Ni_8Nb	306 ± 6
Ni-30Nb	$Ni_{78}Nb_{22}$	↓ Ni-fcc + Ni_3Nb ↑	413 ± 22
Ni-40Nb	$Ni_{70}Nb_{30}$	↑ Ni_3Nb + Ni_6Nb_7 ↓	572 ± 42
Ni-45Nb	$Ni_{66}Nb_{634}$	↓ Ni_3Nb + Ni_6Nb_7 ↑	682 ± 40
Ni-52Nb	$Ni_{60}Nb_{40}$	↓ Ni_3Nb + Ni_6Nb_7 ↑	863 ± 34
Ni-57Nb	$Ni_{55}Nb_{45}$	↓ Ni_3Nb + Ni_6Nb_7 ↑	758 ± 44
Inconel 625	Ni-Cr-Fe-Mo-Nb	Ni-fcc + NbC + $Cr_{23}C_6$	179 – 250

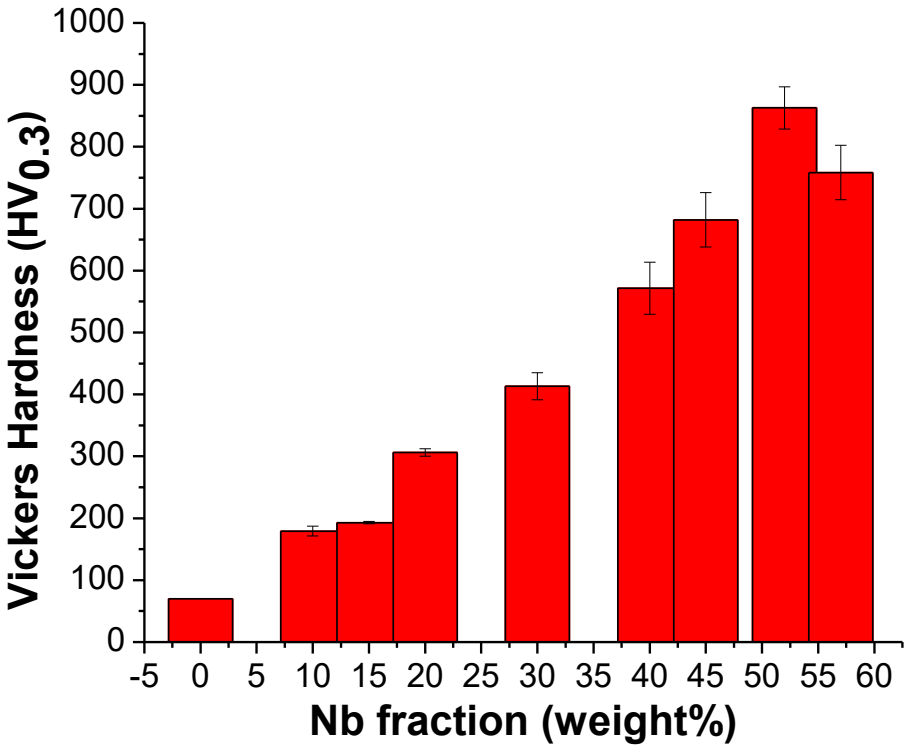

Figure 5: SEM images in BSE mode for copper mold cast (a) Ni-10Nb, (b) Ni-15Nb and (c) Ni-20Nb (wt. %) rapidly solidified alloys.

4. CONCLUSIONS

Ni-Nb binary alloys in a wide range of chemical composition were studied (10, 15, 20, 30, 40, 45, 52 and 57%) since the lack of evidence of crystalline microstructure in the literature. Refinement of γ (Ni-fcc) dendritic microstructure was improved with Nb addition in the Ni-xNb (x = 10, 15, 20 wt.% Nb) alloys together with the formation of higher fraction of the δ-Ni_3Nb intermetallic phase. The presence of needle-like phase SEM image of 20 wt.% Nb suggests the presence of an additional phase different from orthorhombic δ-Ni_3Nb. According to Vickers microhardness measurements of arc-melted Ni-Nb rapidly solidified alloys, showed that in general the higher the Nb content, the higher hardness values, with the exception of 57%Nb, where the hardness dropped, due to the lower fraction of eutectic and the fact that does not present diamond-like precipitated found in 52 wt. %Nb alloy. Interesting changes in microstructure were observed when Nb content increasing, not registered in literature. Further observations must be perform in oreder to observe Ni_8Nb phase.

5. ACKNOWLEDGEMENTS

This work was supported by FAPESP “Projeto Temático” #2013/05987-8 and CNPq in the master´s degree grant of K. Martinez.

6. REFERENCES

Afonso, C.R.M., Bolfarini, C., Botta Filho, W.J., Kiminami, C.S., 2012. Formation and microstructure of Ni62-xNb38Tix (x = 3, 6, 10 at.%) bulk metallic glasses. *International Journal of Materials Research (formerly Z. Metallkd.)* Vol. 103, p. 1096 - 1101.

Afonso, C.R.M., Bolfarini, C., Botta Filho, W.J., Kiminami, C.S., 2007. Spray forming of glass former Fe63Nb10Al4Si3B20 alloy. *Materials Science & Engineering. A, Structural Materials: Properties, Microstructure and Processing*. Vol. 449-451, p. 884.

Catto, F.L., Afonso, C.R.M., Gabriel, A.H.G, Bolfarini, C., Kiminami, C.S., 2017. Rapid solidification and laser cladding of gas atomized Ni-Nb-Sn bulk metallic glass. *Materials Science Forum*, Vol. 899, p.311. doi:10.4028/www.scientific.net/MSF.899.311

Chen, H., Du, Y., Xu, H., Schuster, J.C., 2006. "Refinement of the thermodynamic modeling of the Nb–Ni". *Computer Coupling of Phase Diagrams and Thermochemistry*, Vol. 30, p. 308-315.

Davis, J.R., 2000. *ASM Specialty Handbook, Nickel, Cobalt and their Alloys*. ASM International, Materials Park, Ohio, 1st edition.

Donachie, J.M., Donachie, J.S., 2002. *Superalloys, a Technical guide.* ASM International, Materials Park, Ohio, 2nd edition.

Gargarella P., Almeida A., Vilar R., Afonso C.R.M., Peripolli S., Rios C.T., Bolfarini C., Botta Filho W.J., Kiminami, C.S., 2014. Formation of Fe-based glassy matrix composite coatings by laser processing. *Surface Coatings and Technology*. Vol. 240, p. 336.

Inoue, A., Masumoto, T., Furukawa, S., Chen, H.S. 1988. Preparation of Fe-, Co-, and Ni-Based amorphous alloy powders by high-pressure gas atomization and their structural relaxation behavior. *Metallurgical Transactions A*, Vol. 19, p. 235.

Inoue, A., Suryanarayana, C., 2011. *Bulk Metallic Glasses.* CRC Press, New York, 1st edition.

Koch, C.C., Cavin, O.B., McKamey, C.G., W., Scarbrough, J.O., 1983. "Preparation of amorphous $Ni_{60}Nb_{40}$ by mechanical alloying ". *Applied Phisics Letters* Vol. 43, p.1017.

Leonhardt, M., Löser, W., Lindenkreuz, H.G., 1999. "Solidification kinetics and phase formaton of undercooled eutectic Ni-Nb melts". *Acta Meterialia*, Vol. 47, p. 2961-2968.

May, José E.; Oliveira, Marcelo F.; Afonso, C. R. M.; Lisboa, R. D. S.; Kuri, S. E., 2004. Amorphous phase partitioning in FeCo-based metallic glass alloys. *Journal of Non-Crystalline Solids*, Vol. 348, p. 250 - 257.

Minouei, H., Akbari, G.H., Enayati, M.H., Hong, S.I., 2017. "Amorphization and nanocrystallization of Ni-Nb-Si alloys". *Materials Science & Engineering*, Vol. 682, p. 396-401.

Special Metals 2013. *Inconel® 625.* Special Metals Corporation.Available: www.specialmetals.com

Special Metals 2013. *Inconel® 718.* Special Metals Corporation. Available: www.specialmetals.com

Zhang, L.; Zhuo, M.-J.; Xu, J. 2011. Enhancing bulk metallic glass formation in Ni–Nb–Sn-based alloys via substitutional alloying with Co and Hf. *Journal of Materials Research*, Vol. 23 (3), p. 688–699.

7. RESPONSIBILITY NOTICE

The author(s) is (are) the only responsible for the printed material included in this paper.